Cosmic Microwave Background Overview

J. Richard Bond

CIAR Cosmology Program, Canadian Institute for Theoretical Astrophysics, 60 St. George St., Toronto, ON M5S 3H8, Canada

Abstract. The goal of CMB and large scale structure (LSS) research is to determine the cosmological parameters that define how structure arose in the universe. These include: early universe parameters associated with fluctuation generation, such as their statistics, and the amplitude and shape of primordial power spectra, and the topology of space to the extent that this is accessible; the densities of the various species present, baryons, cold and hot dark matter, the vacuum, as well as the overall mean curvature of space. Current CMB and LSS data provide strong support for the gravitational instability theory, rule out cosmic explosions as a dominant source of LSS, suggest that there was a long period in which hydrogen was recombined between the redshift of photon decoupling and reionization associated with early object formation, and are consistent with inflation-based expectations. For example, for inflation-based Gaussian fluctuations in a tilted ΛCDM sequence, the slope of the initial spectrum is within about 5% of the (preferred) scale invariant form both when just the CMB data is used, and when it is combined with LSS data; with both, a nonzero value of Ω_Λ is strongly preferred. The corresponding *o*CDM tilted open sequence prefers $\Omega_{tot} < 1$, but is overall less likely than the flat $\Omega_\Lambda \neq 0$ sequence. Forecasts of future balloon and satellite experiments predict percent-level accuracy will be attainable among a large fraction of the 10+ parameters characterizing the cosmic structure formation theory.

PACS numbers: xxx,xxx

1. What We Can Learn From the CMB and LSS

A broad visual overview of the different probes we use to try to pin down the amplitude of density and gravitational metric fluctuations as a function of length scale is shown in Fig. 1. The measure of length is comoving Fourier wavenumber $k = 2\pi\bar{a}/\lambda$, with the cosmological scale factor $\bar{a}(t)$ removed from the physical wavelength $\lambda(t)$. The length unit is the h^{-1} Mpc, where h is the Hubble parameter in units of 100 km s^{-1} Mpc^{-1}, *i.e.*, really a velocity unit. Until a few years ago h was considered to be uncertain by a factor of two or so, but is now thought to be between 0.6 and 0.7. For compact spatial manifolds, the wavenumbers have an initially discrete spectrum, and are missing ultralong waves, limited by the size of the manifold. Although the scales we can probe most effectively are smaller than the size of our Hubble patch ($\sim 3000\,\mathrm{h}^{-1}$ Mpc), because ultralong waves contribute gentle gradients to CMB observables, we can in fact place useful constraints on the ultralarge scale structure (ULSS) realm "beyond our horizon". Indeed current constraints on the size of the universe arise partly from this region and partly from the very large scale structure (VLSS) region.

The COBE data and CMB experiments with somewhat higher resolution probe the VLSS region very well. Density fluctuations are highly linear in that regime, which

is what makes it so simple to analyze. One of the most interesting realms is the LSS one, in which CMB observations probe exactly the scales that LSS redshift surveys probe. The density fluctuations are linear to weakly nonlinear in this realm, so we can still interpret the LSS observations reasonably well — with one important caveat: Galaxies form and shine through complex nonlinear dissipative processes, so how they are distributed may be rather different than how the total mass is distributed. The evidence so far is consistent with this "bias" being only a linear amplifier of the mass fluctuations on large scales, albeit a different one for different galaxy types. Detailed comparison of the very large CMB and LSS redshift survey results we will get over the next five years should help enormously in determining the statistical nature of the bias.

Within the LSS band, important scales for the CMB arise: the sound crossing distance at photon decoupling around redshift 1000, $\sim 100\,\mathrm{h}^{-1}$ Mpc; the width of the region over which this decoupling occurs, which is about a factor of 10 smaller, and below which primary CMB anisotropies are damped.

The length scales below LSS, labelled "gastrophysics", are ones over which energy injection and propagation, through ionization and shock fronts from galaxies, quasars, etc. are expected to have had important effects. Although probes based on catalogues of high redshift galaxies and quasars, and on quasar absorption lines from the intergalactic medium, represent a very exciting observational frontier, it will be difficult for theoretical conclusions about the early universe and the underlying fluctuations to be divorced from these gastrophysical complications.

1.1. CMB as a Probe of Early Universe Physics

The source of fluctuations to input into the cosmic structure formation problem is likely to be found in early universe physics. We want to measure the CMB (and large scale structure) response to these initial fluctuations. The goal is the lofty one of peering into the physical mechanism by which the fluctuations were generated. The contenders for generation mechanism are (1) "zero point" quantum noise in scalar and tensor fields that must be there in the early universe if quantum mechanics is applicable and (2) topological defects which may arise in the inevitable phase transitions expected in the early universe.

From CMB and LSS observations we hope to learn: the statistics of the fluctuations, whether Gaussian or non-Gaussian; the mode, whether adiabatic or isocurvature scalar perturbations, and whether there is a significant component in gravitational wave tensor perturbations; the power spectra for these modes, $\mathcal{P}_\Phi(k), \mathcal{P}_{is}(k), \mathcal{P}_{GW}(k)$ as a function of comoving wavenumber k. Sample initial and evolved power spectra for the gravitational potential $\mathcal{P}_\Phi(k)$ ($\equiv d\sigma_\Phi^2/d\ln k$, the *rms* power in each $d\ln k$ band) are shown in Fig. 1. As the Universe evolves the initial shape of $\mathcal{P}_\Phi$ (nearly flat or scale invariant) is modified by characteristic scales imprinted on it that reflect the values of cosmological parameters such as the energy densities of baryons, cold and hot dark matter, in the vacuum (cosmological constant), and in curvature. Many observables can be expressed as weighted integrals over k of the power specta and thus can probe both density parameters and initial fluctuation parameters.

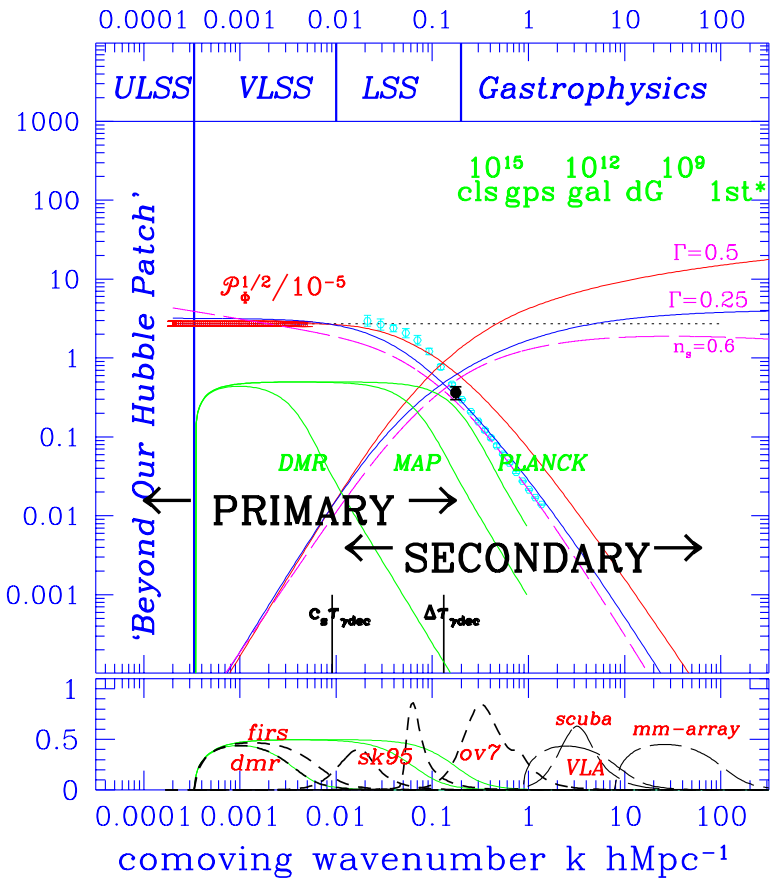

Figure 1. The bands in comoving wavenumber k probed by CMB primary and secondary anisotropy experiments, in particular by the satellites COBE, MAP and Planck, and by large scale structure (LSS) observations are contrasted. The width of the CMB photon decoupling region and the sound crossing radius ($\Delta\tau_{\gamma dec}, c_s\tau_{\gamma dec}$) define the effective acoustic peak range for primary anistropies (those involving linear fluctuations). Secondary anisotropies arise only once matter has gone nonlinear. Sample (linear) gravitational potential power spectra (actually $\mathcal{P}_\Phi^{1/2}(k)$) are also plotted, and the y-axis values refer to $\mathcal{P}_\Phi^{1/2}/10^{-5}$ (which is dimensionless). The horizontal dotted line is the post-inflation scale invariant power spectrum, which is bent down as the universe evolves by an amount dependent upon the matter content. The hatched region at low k gives the 4 year DMR error bar on the Φ amplitude in the COBE regime. The solid data point in the cluster-band denotes the Φ constraint from the abundance of clusters (for Ω_{tot}=1,Ω_Λ=0). The open circles are estimates of the linear Φ power from current galaxy clustering data by [5]. A bias is "allowed" to (uniformly) raise the shapes to match the observations. The corresponding linear density power spectra, $\mathcal{P}_\rho^{1/2}(k)$, are also shown rising to high k: Models are the "standard" $n_s = 1$ CDM model (labelled $\Gamma = 0.5$ with $\Omega_{nr} = 1$, h = 0.5), a tilted ($n_s = 0.6$, $\Gamma = 0.5$) CDM model and a model with the shape modified ($\Gamma = 0.25$) by changing the matter content of the Universe, *e.g.*, $\Omega_{nr} = 0.36$, h = 0.7. As the universe evolves, $\mathcal{P}_\rho^{1/2}(k)$ grows from small values with redshift until it crosses unity at small scales, and the first star forming tiny dwarf galaxies appear ("1st *"), typically at redshift about 20; k_{NL} decreases with time, leaving in its wake dwarf galaxies (dG), normal galaxies (gal), groups (gps) and clusters (cls), forming from waves concentrated in the k-space bands that their labels cover. Equivalent mass scales are given above them. Because the $\mathcal{P}_\Phi$ of the COBE-normalized sCDM model shown shoots high relative to the cluster data point, the sCDM model is strongly ruled out. More rigorous discussion of what is compatible with COBE, smaller angle CMB experiments such as SK95, the cluster data point and the shape of the $\mathcal{P}_\Phi$ spectrum as estimated from galaxy clustering data is given in § 2.3. The filter functions plotted for SK95, Planck, etc. show the bands they are sensitive to: multiplying by a k-space $\Delta T/T$ power spectrum gives the variance per $\ln k$).

1.2. Cosmic Structure and the Nonlinear Wavenumber

The (linear) density power spectra, $\mathcal{P}_\rho(k) \propto k^4\mathcal{P}_\Phi(k)$, are also shown in Fig. 1. In hierarchical structure formation models such as those considered here, the nonlinear wavenumber $k_{NL}(t)$, defined by $\int_0^{k_{NL}} \mathcal{P}_\rho(k) d\ln k$=1, grows as the universe expands. $k_{NL}(t)$ was in the galaxy band at redshift 3 and is currently in the cluster band.

At a given time t, there is a band in k extending just above $k_{NL}(t)$ which is primarily responsible for the nonlinear collapsed dark matter halos in the medium in hierarchical theories. Smaller halos that formed earlier from much higher k bands would have largely merged into the halos of relevance at epoch t. The reason galaxies are still around today when k_{NL} is cluster scale is that, although the outer halos of the galaxies will have largely merged, gas cooling allows the baryons and some of the dark matter to concentrate and survive as independent beings in groups and clusters.

Scales just below k_{NL} are weakly nonlinear and define the characteristic patterns of filaments connecting clusters, and membranes connecting filaments. Voids are rare density minima which have opened up by gravitational dynamics and merged, opposite to the equally abundant rare density maxima, the clusters, in which the space collapses by factors of 5-10 and more.

At $k > k_{NL}(t)$, nonlinearities and complications associated with dissipative gas processes can obscure the direct connection to the early universe physics. Most easily interpretable are observables probing the linear regime now, $k < k_{NL}(t_0)$. CMB anisotropies arising from the linear regime are termed primary; as Fig. 1 shows, these probe 3 decades in wavenumber. LSS observations at low redshift probe a smaller, but overlapping, range. We have hope that $z \sim 3$ LSS observations, when $k_{NL}(t)$ was larger, can extend the range, but gasdynamics can modify the relation between observable and power spectrum in complex ways. Secondary anisotropies of the CMB (§ 1.7), those associated with nonlinear phenomena, also probe smaller scales and the "gastrophysical" realm.

1.3. Cosmic Parameters

Even simple Gaussian inflation-generated fluctuations for structure formation have a large number of early universe parameters we would wish to determine (§ 1.4): power spectrum amplitudes at some normalization wavenumber k_n for the modes present, $\{\mathcal{P}_\Phi(k_n), \mathcal{P}_{is}(k_n), \mathcal{P}_{GW}(k_n)\}$; shape functions for the "tilts" $\{\nu_s(k), \nu_{is}(k), \nu_t(k)\}$, usually chosen to be constant or with a logarithmic correction, e.g., $\nu_s(k_n), d\nu_s(k_n)/d\ln k$. (The scalar tilt for adiabatic fluctuations, $\nu_s(k) \equiv d\ln\mathcal{P}_\Phi/d\ln k$, is related to the usual index, n_s, by $\nu_s = n_s - 1$.) The transport problem (§ 1.6) is dependent upon physical processes, and hence on physical parameters. A partial list includes the Hubble parameter h, various mean energy densities $\{\Omega_{tot}, \Omega_B, \Omega_\Lambda, \Omega_{cdm}, \Omega_{hdm}\}\mathrm{h}^2$, and parameters characterizing the ionization history of the Universe, e.g., the Compton optical depth τ_C from a reheating redshift z_{reh} to the present. Instead of Ω_{tot}, we prefer to use the curvature energy parameter, $\Omega_k \equiv 1 - \Omega_{tot}$, thus zero for the flat case. In this space, the Hubble parameter, $\mathrm{h} = (\sum_j(\Omega_j\mathrm{h}^2))^{1/2}$, and the age of the Universe, t_0, are functions of the $\Omega_j\mathrm{h}^2$. The density in nonrelativistic (clustering) particles is $\Omega_{nr} = \Omega_B + \Omega_{cdm} + \Omega_{hdm}$. The density in relativistic particles, Ω_{er}, includes photons, relativistic neutrinos and decaying particle products, if any. Ω_{er}, the abundance of primordial helium, etc. should also be considered as parameters to be determined. The count is thus at

least 17, and many more if we do not restrict the shape of $\mathcal{P}_\Phi(k)$ through theoretical considerations of what is "likely" in inflation models. Estimates of errors on a smaller 9 parameter inflation set for the MAP and Planck satellites are given in § 2.4.

The arena in which CMB theory battles observation is the anisotropy power spectrum in multipole space, Fig. 3, which shows how primary $\mathcal{C}_\ell$'s vary with some of these cosmic parameters. Here $\mathcal{C}_\ell \equiv \ell(\ell+1)\langle|(\Delta T/T)_{\ell m}|^2\rangle/(2\pi)$. The $\mathcal{C}_\ell$'s are normalized to the 4-year *dmr*(53+90+31)(A+B) data [3, 1, 4]. The arena for LSS theory battling observations is the $\mathcal{P}_\Phi$ of Fig. 1. (Usually it is $\mathcal{P}_\rho/k^3 \sim k\mathcal{P}_\Phi$ which is plotted.)

For a given model, the early universe $\mathcal{P}_\Phi$ is uniquely related to late-time power spectrum measures of relevance for the CMB, such as the quadrupole $\mathcal{C}_2^{1/2}$ or averages over ℓ-bands B, $\langle\mathcal{C}_\ell\rangle_B^{1/2}$, and to LSS measures, such as the *rms* density fluctuation level on the $8\,h^{-1}$ Mpc (cluster) scale, σ_8, so any of these can be used in place of the primordial power amplitudes in the parameter set. In inflation, the ratio of gravitational wave power to scalar adiabatic power is $\mathcal{P}_{GW}/\mathcal{P}_\Phi \approx -(100/9)\nu_t/(1-\nu_t/2)$, with small corrections depending upon $\nu_s - \nu_t$ [1, 2]. If such a relationship is assumed, the parameter count is lowered by one.

1.4. Freedom in Inflation

Many variants of the basic inflation theme have been proposed, sometimes with radically different consequences for $\mathcal{P}_\Phi(k) \sim k^{1-n_s(k)}$, and thus for the CMB sky, which is used in fact to highly constrain the more baroque models. A rank-ordering of inflation possibilities (see e.g., [1, 2, 6] for references): (1) adiabatic curvature fluctuations with nearly uniform scalar tilt over the observable range, slightly more power to large scales ($0.8 \lesssim n_s \lesssim 1$) than "scale invariance" ($n_s = 1$) gives, a predictable nonzero gravity wave contribution with tilt similar to the scalar one, and tiny mean curvature ($\Omega_{tot} \approx 1$); (2) same as (1), but with a tiny gravity wave contribution; (3) same as (1) but with a subdominant isocurvature component of nearly scale invariant tilt (the case in which isocurvature dominates is ruled out); (4) radically broken scale invariance with weak to moderate features (ramps, mountains, valleys) in the fluctuation spectrum (strong ones are largely ruled out); (5) radical breaking with non-Gaussian features as well; (6) "open" inflation, with quantum tunneling producing a negatively-curved (hyperbolic) space which inflates, but not so much as to flatten the mean curvature ($d_c \sim (Ha)^{-1}$, not $\gg (Ha)^{-1}$, where $d_c \equiv H_0^{-1}|\Omega_k|^{-1/2}$); (7) quantum creation of compact hyperbolic space from "nothing" with volume d_T^3 which inflates, with $d_T \sim (Ha)^{-1}$, not $\gg (Ha)^{-1}$, and d_T of order d_c; (8) flat ($d_c = \infty$) inflating models which are small tori of scale d_T with d_T a few $(Ha)^{-1}$ in size. It is quite debatable which of the cases beyond (2) are more or less plausible, with some claims that (4) is supersymmetry-inspired, others that (6) is not as improbable as it sounds. Of course, how likely *a priori* the cases (7) and (8) of most concern to us here is completely unknown, but it is the theorists' job to push out the boundaries of the inflation idea and use the data to select what is allowed.

1.5. LSS Constraints on the Power Spectrum

We have always combined CMB and LSS data in our quest for viable models. Fig. 1 shows how the two are connected. DMR normalization precisely determines σ_8 for each model considered; comparing with the $\sigma_8 \sim 0.6\Omega_{nr}^{-0.56}$ target value derived from cluster

abundance observations severely constrains the cosmological parameters defining the models. In Fig. 1, this means the COBE-normalized $\mathcal{P}_\Phi(k)$ must thread the "eye of the needle" in the cluster-band.

Similar constrictions arise from galaxy-galaxy and cluster-cluster clustering observations: the shape of the linear $\mathcal{P}_\Phi$ must match the shape reconstructed from the data. The reconstruction shown is from [5]. The clustering observations are roughly compatible with an allowed range $0.15 \lesssim \Gamma + \nu_s/2 \lesssim 0.3$, where $\Gamma \approx \Omega_{nr}\,\mathrm{h}\,[\Omega_{er}/(1.68\Omega_\gamma)]^{-1/2}\,e^{-(\Omega_B(1+\Omega_{nr}^{-1}(2\mathrm{h})^{1/2})-0.06)}$ characterizes the density transfer function shape. The sCDM model has $\Gamma \approx 0.5$. To get $\Gamma + \nu_s/2$ in the observed range one can: lower h, lower Ω_{nr} (ΛCDM, oCDM), raise Ω_{er}, the density parameter in relativistic particles ($1.68\Omega_\gamma$ with 3 species of massless neutrinos and the photons), e.g., as in τCDM, with a decaying ν of lifetime τ_d and $\Gamma \approx 1.08\Omega_{nr}\mathrm{h}(1 + 0.96(m_\nu\tau_d/\mathrm{keV\ yr})^{2/3})^{-1/2}$; raise Ω_B; tilt $\nu_s < 0$ (tCDM), for standard CDM parameters, e.g., $0.3 \lesssim n_s \lesssim 0.7$ would be required. Adding a hot dark matter component gives a power spectrum characterized by more than just Γ. In the post-COBE era, all of these models that lower $\Gamma+\nu_s/2$ have been under intense investigation to see which survive as the data improves, if any.

1.6. Cosmological Radiative Transport

Cosmological radiative transfer is on a firm theoretical footing. For reviews, see [1, 7, 8]. Together with a gravity theory (invariably Einstein's general relativity, but the CMB will eventually be used as a test of the gravity theory) and the transport theory for the other fields and particles present (baryons, hot, warm and cold dark matter, coherent fields, i.e., "dynamical" cosmological "constants", *etc.*), we propagate initial fluctuations from the early universe through photon decoupling into the (very) weakly nonlinear phase, and predict *primary anisotropies*, those calculated using either linear perturbation theory (e.g., for inflation-generated fluctuations), or, in the case of defects, linear response theory. The sources driving their development are all proportional to the gravitational potential Φ: the "naive" Sachs-Wolfe effect, $\Phi/3$; photon bunching and rarefaction (acoustic oscillations), $\frac{1}{4}\frac{\delta\rho_\gamma}{\rho_\gamma}$, responsible for the adiabatic $\frac{1}{3}\frac{\delta\rho_B}{\rho_B}$ effect and the isocurvature effect; linear-order Thompson scattering (Doppler), $\sigma_T\bar{n}_e\mathbf{v}_e\cdot\hat{q}$, with σ_T the Thomson cross section, $\mathbf{v}_e$ and $\bar{n}_e$ the electron velocity and density, and $\hat{q}$ the photon direction; the (line-of-sight) integrated Sachs-Wolfe effect, $\sim 2\int_{l.o.s.}\dot{\Phi}$; there are also subdominant anisotropic stress and polarization terms. For primary tensor anisotropies, the sources are the two polarization states of gravity waves, $\frac{1}{2}\dot{h}_{+,\times}$; again there are subdominant polarization terms.

Spurred on by the promise of percent-level precision in cosmic parameters from CMB satellites (§ 2.4), a considerable fraction of the CMB theoretical community with Boltzmann transport codes compared their approaches and validated the results to ensure percent-level accuracy up to $\ell \sim 3000$ (COMBA [9]). An important goal for COMBA was speed, since the parameter space we wish to constrain has many dimensions. Most groups have solved cosmological radiative transport by evolving a hierarchy of coupled moment equations, one for each ℓ. Although the equations and techniques were in place prior to the COBE discovery for scalar modes, and shortly after for tensor modes, to get the high accuracy with speed has been somewhat of a challenge. There are alternatives to the moment hierarchy for the transport of

photons and neutrinos. In particular the entire problem of photon transport reduces to integral equations in which the multipoles with $\ell > 2$ are expressed as history-integrals of metric variables, photon-bunching, Doppler and polarization sources. The fastest COMBA-validated code, "CMBfast", uses this method [10] and is publicly available.

1.7. Secondary Anisotropies

Although hydrodynamic and radiative processes are expected to play important roles around collapsed objects and may bias the galaxy distribution relative to the mass (*gastrophysics* regime in Fig. 1), a global role in obscuring the early universe fluctuations by late time generation on large scales now seems unlikely. Not too long ago it seemed perfectly reasonable based on extrapolation from the physics of the interstellar medium to the pregalactic and intergalactic medium to suppose hydrodynamical amplification of seed cosmic structure could create the observed Universe. The strong limits on Compton cooling from the COBE FIRAS experiment [11], in energy $\delta E_{Compton\ cool}/E_{cmb} = 4y < 6.0 \times 10^{-5}$ (95% CL), constrain the product $f_{exp} R_{exp}^2$ of filling factor f_{exp} and bubble formation scale R_{exp}, to values too small for a purely hydrodynamic origin. If supernovae were responsible for the blasts, the accompanying presupernova light radiated would have been much in excess of the explosive energy (more than a hundred-fold), leading to much stronger restrictions (e.g., [1]).

Nonetheless significant "secondary anisotropies" are expected. These include: linear weak lensing, dependent on the 2D tidal tensor, a projection of the 3D tidal tensor $\partial^2\Phi/\partial x^i \partial x^j$; the Rees-Sciama effect, $2\int_{l.o.s.} \dot{\Phi}_{NL}$, dependent upon the gravitational potential changes associated with nonlinear structure formation; nonlinear Thompson scattering, $\sigma_T \delta n_e \mathbf{v}_e \cdot \hat{q}$, dependent upon the fluctuation in the electron density δn_e as well as $\mathbf{v}_e$, and responsible for the quadratic-order (Vishniac) effect and the "kinematic" Sunyaev-Zeldovich (SZ) effect (moving cluster/galaxy effect); the thermal SZ effect, associated with Compton cooling, $\int_{l.o.s.} \psi_K(x)\delta(n_e T_e)$, where $\psi_K(x)$ is a function of $x = E_\gamma/T_\gamma$ passing from -2 on the Rayleigh-Jeans end to x on the Wein end, with a null at $x = 2.83$ (i.e., 1863μm or 161 GHz); pregalactic or galactic dust emission, $\sim \int_{l.o.s.} \psi_{dust}(x_d)\rho_d$, dependent upon the distribution of the dust density ρ_d and temperature T_d through a function ψ_{dust} of $x_d = E_\gamma/T_d$.

Secondary anisotropies may be considered as a nuisance foreground to be subtracted to get at the primary ones, but they are also invaluable probes of shorter-distance aspects of structure formation theories, full of important cosmological information. The k-space range they probe is shown in Fig. 1. The effect of lensing is to smooth slightly the Doppler peaks and troughs of Fig. 3. $\mathcal{C}_\ell$'s from quadratic nonlinearities in the gas at high redshift are concentrated at high ℓ, but for most viable models are expected to be a small contaminant. Thomson scattering from gas in moving clusters also has a small effect on $\mathcal{C}_\ell$ (although it should be measurable in individual clusters). Power spectra for the thermal SZ effect from clusters are larger [12]; examples in the top panel of Fig. 3 are for untilted $H_0 = 70$ COBE-normalized ΛCDM and oCDM models, with $\bar{y} \sim 2 \times 10^{-6}\,(\Omega_B h^2/0.025)$, and a cluster-normalized sCDM model, with $\bar{y} \sim 0.8 \times 10^{-6}$, still small *c.f.* the FIRAS constraint. Although $\mathcal{C}_\ell^{(SZ)}$ may be small, because the power for such non-Gaussian sources is concentrated in hot or cold spots the signal is detectable, in fact has been for two dozen clusters now at the > 5 sigma level, and indeed the SZ effect will soon be usable for cluster-finding.

$\mathcal{C}_\ell$ for a typical dusty primeval galaxy model is concentrated at higher ℓ associated with galaxy sizes, although a small contribution associated with clustering extends into the lower ℓ range. These dusty anisotropies are now observable with instrumentation on submm telescopes (e.g., SCUBA on the James Clerk Maxwell Telescope on Mauna Kea).

2. CMB Parameter Estimation, Current and Future

We have progressed from the tens of pixels of early $\Delta T/T$ experiments through thousands for DMR [3] and SK95 [13], soon tens of thousands for long duration balloon experiments (LDBs) and eventually millions for the MAP [14] and Planck [15] satellites. Finding nearly optimal strategies for data projection, compression and analysis which will allow us to disentangle the primary anisotropies from the Galactic and extragalactic foregrounds and from the secondary anisotropies induced by nonlinear effects will be the key to realizing the theoretically-possible precision on cosmic parameters and so to determine the winners and losers in theory space. Particularly powerful is to combine results from different CMB experiments and combine these with LSS and other observations. Application of the same techniques to demonstrate self-consistency and cross-consistency of experimental results is essential for validating conclusions drawn from the end-product of data analysis, *e.g.*, the power spectra in bands as shown in Fig. 3 and the cosmic parameters they imply.

Current band-powers are shown in the upper panel of Fig. 3. It is possible that some of the results may still include residual signals, but it is encouraging that completely different experiments with differing frequency coverage give similar bandpowers. Lower panels compress the information into 9 optimal bandpower estimates derived from all of the current data by Jaffe, Knox and I. The first lesson of Fig. 3 is that, in broad brush stroke, smaller angle CMB data (e.g., SP94, SK95, MSAM, MAX) are consistent with COBE-normalized $\mathcal{C}_\ell$'s for the untilted inflation-based models.

The few data points below $\ell \lesssim 20$ are mainly from COBE's DMR experiment. Clearly the ℓ-range spanned by DMR is not large enough to fix well the cosmological parameter variations shown in the right panels, but combining CMB anisotropy experiments probing different ranges in ℓ-space improves parameter estimates enormously because of the much extended baseline: it is evident that n_s can be reasonably well determined, low Ω open models violate the data, but Ω_Λ cannot be well determined by the CMB alone.

2.1. DMR and Constraints on Ultra-large Scale Structure

DMR is fundamental to analyses of the VLSS region and ULSS region, and is the data set that is the most robust at the current time. The average noise in the 53+90+31 GHz map is about $20\mu K$ per *fwhm* beam ($\sim 7^\circ$), and there are about 700 of these resolution elements outside of the Galactic disk cut (about 4000 2.6° DMR pixels with $60\mu K$ noise). The signal is about $37\mu K$ per beam: i.e., there is a healthy signal-to-noise ratio. The signal-to-noise for widespread modes (e.g., multipoles with $\ell \lesssim 15$) is even better. Indeed, even with the much higher precision MAP and Planck experiments we do not expect to improve the results on the COBE angular scales greatly because the 4-year COBE data has sufficiently large signal-to-noise that one is almost in the cosmic variance error limit (due to realization to realization fluctuations

of skies in the theories) which cannot be improved upon no matter how low the experimental noise.

Wiener-filtered maps shown in Fig. 2.1 give the statistically-averaged signal given the data and a best-fit signal model. These optimally-filtered maps are insensitive to modest variations in the assumed theory. The robustness of features in the maps as a function of frequency and the weak frequency dependence in the bandpowers are strong arguments that what is observed is on the sky with a primary anisotropy origin, made stronger by the compatible amplitudes and positive cross-correlations with the FIRS and Tenerife data sets.

Recall the "beyond our horizon" land in Fig. 1 is actually partly accessible because long waves contribute gentle gradients to our observables. The DMR data is well suited to probe this regime. Constraints on such "global parameters" as average curvature from COBE are not very good. Obviously it is much preferred to use the smaller angle data on the acoustic peak positions. The COBE data can be used to test whether radical broken scale results in a huge excess or deficit of power in the COBE k-space band, *e.g.*, just beyond $k^{-1} \sim H_0^{-1}$, but this has not been much explored. The remarkable non-Gaussian structure predicted by stochastic inflation theory would likely be too far beyond our horizon for its influence to be felt. The bubble boundary in hyperbolic inflation models may be closer and its influence shortly after quantum tunneling occurred could possibly have observable consequences for the CMB. Theorists have also constrained the scale of topology in simple models (Fig. 2.1). We [23] find the torus scale is $d_T/2 > 1.1(2H_0^{-1}) = 6600\,\mathrm{h}^{-1}$ Mpc from DMR for flat equal-sided 3-tori at the 95% confidence limit, slightly better than other groups find since we used full map statistics. The constraint is not as strong if the repetition directions are asymmetric, $> 0.7(2H_0^{-1})$ for 1-tori from DMR. It is also not as strong if more general topologies are considered, e.g., the large class of compact hyperbolic topologies [23, 24].

2.2. Cosmic Parameters from All Current CMB Data

Jaffe and I [4] have undertaken full Bayesian statistical analysis of the 4 year DMR [3], SP94 [16] and SK94/SK95 [17, 13] data sets, taking into account all correlations among pixels in the data and theory. Other experiments were included by using their bandpowers as independent points with the Gaussian errors shown in Fig. 3. We have shown this approximate method works reasonably well by comparing results derived for DMR+SP94+SK95 with the full analysis with those using just their bandpowers [20]. Other groups have also calculated parameter constraints using the bandpower approach [37].

With current errors on the data, simultaneously exploring the entire parameter space of § 1.3 is not useful, so we restricted our attention to various subregions of $\{\Omega_B\mathrm{h}^2, \Omega_{cdm}\mathrm{h}^2, \Omega_{hdm}\mathrm{h}^2, \Omega_k\mathrm{h}^2, \Omega_\Lambda\mathrm{h}^2, \nu_s, \nu_t, \sigma_8\}$, such as $\{\sigma_8, n_s, \mathrm{h}\,|\,\mathrm{fixed}\,t_0, \Omega_B\mathrm{h}^2\}$, where Ω_k=0 and Ω_Λ is a function of $\mathrm{h}t_0$ or Ω_Λ=0 and $\Omega_k > 0$ is a function of $\mathrm{h}t_0$. The age of the Universe, t_0, was chosen to be 11, 13 or 15 Gyrs. A recent estimate for globular cluster ages with the Hipparcos correction is 11.5 ± 1.3 Gyr [22], with perhaps another Gyr to be added associated with the delay in globular cluster formation, so 13 Gyr is a good example. We considered the ranges $0.5 \le n_s \le 1.5$, $0.43 \le \mathrm{h} \le 1$, and $0.003 \le \Omega_B\mathrm{h}^2 \le 0.05$. The old "standard" nucleosynthesis estimate was $\Omega_B\mathrm{h}^2 = 0.0125$, but the preferred one is now 0.025. We assumed reheating occurred sufficiently late to have a negligible effect on $\mathcal{C}_\ell$, by no means clear. $\mathcal{C}_\ell$'s for

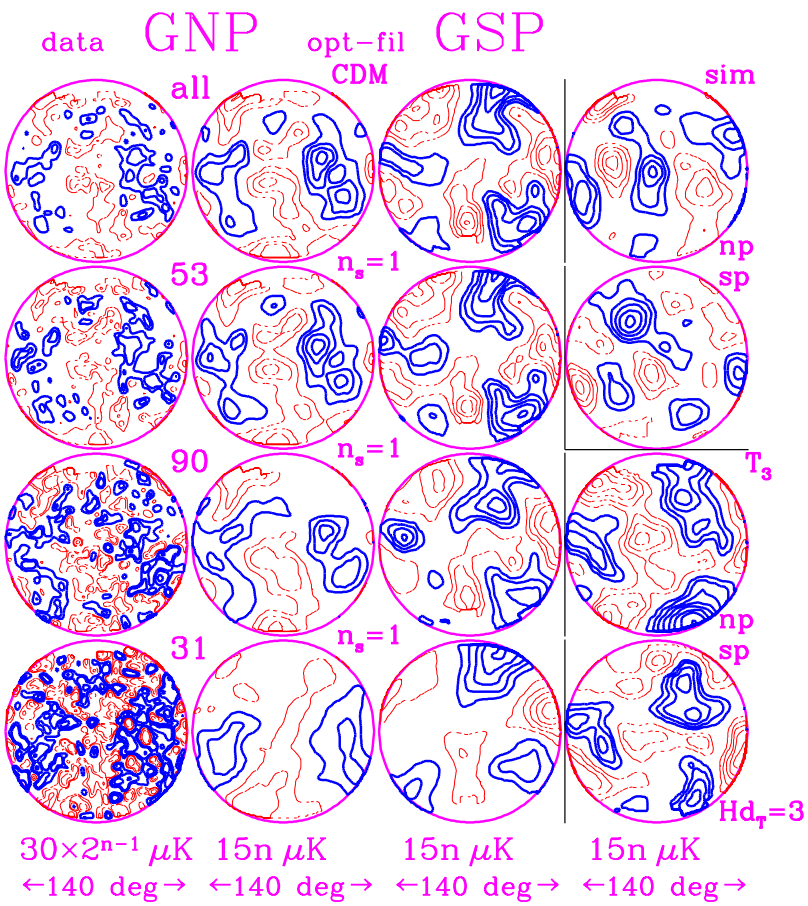

Figure 2. The first column shows unfiltered 140° diameter *dmr* $A+B$ maps centered on the North Galactic Pole, the second shows them after Wiener-filtering (with monopole, dipole and quadrupole removed), the third the South Pole version, with the *nth* contour as noted and negative contours heavier than positive ones. The Wiener maps use a model which fits the correlation function and amplitude of the DMR data (specifically, the n_s=1 sCDM model was used, but insensitive to even rather significant variations). The maps have been smoothed by a 1.7° Gaussian filter. *all* is $53+90+31A+B$. Although higher noise results in filtering on greater angular scales, the large scale features of all maps are the same. This is also borne out by detailed statistical comparisons map to map. The last column shows some theoretical realizations, after optimal filtering. The first two rows are the NGP and SGP for a n_s=1 CDM model. The lower two rows are for a 3-torus topology, with repetition length $d_T = 9000\,\mathrm{h}^{-1}$ Mpc, 1.5 times the horizon radius, in all three directions, a model strongly ruled out because of the high degree of positive correlation between the North and Southern hemispheres that the periodicity induces. Highly correlated patterns also exist for small compact hyperbolic models.

sample restricted parameter sequences are shown in Fig. 3. We made use of signal-to-noise compression of the data (by factors of 3) in order to make the calculations of likelihood functions such as $\mathcal{L}(\sigma_8, n_s, \mathrm{h} \,|\, \mathrm{fixed}\, t_0, \Omega_B \mathrm{h}^2)$ more tractable (without loss of information or accuracy).

The n_s constraints are quite good. If σ_8 is marginalized for the tilted ΛCDM sequence with H_0=50, with DMR only the primordial index is $n_s = 1.02^{+.23}_{-.25}$ with no gravity waves, ν_t=0 and $1.02^{+.23}_{-.18}$ with gravity waves and ν_t=ν_s, rather encouraging for the nearly scale invariant models preferred by inflation theory. For the 13 Gyr tilted ΛCDM sequence, when all of the current CMB data are used we get $1.02^{+.05}_{-.03}$ for $H_0 = 50$ (and $\Omega_\Lambda = 0$, the tilted sCDM model sequence) and $1.00^{+.04}_{-.04}$ for $H_0 = 70$ (and $\Omega_\Lambda = 0.66$). Marginalizing over H_0 gives $1.01^{+.05}_{-.04}$ with gravity waves included, $0.98^{+.08}_{-.06}$ if they are not. The marginalized 13 Gyr tilted oCDM sequence gives $1.00^{+.05}_{-.05}$.

H_0 and Ω_Λ for fixed age are not that well determined by the CMB data alone. After marginalizing over all n_s, we get $H_0 < 75$ at 1σ, but effectively no constraint at 2σ. The strong dependence of the position of the acoustic peaks on Ω_k means that the oCDM sequence is better restricted: $\Omega_{tot} \sim .7$ is preferred; for the 13 Gyr sequence this gives $H_0 \approx 53$ and for the 11 Gyr sequence $H_0 \approx 65$.

Calculations of defect models (*e.g.* strings and textures) give $\mathcal{C}_\ell$'s that do not have the prominent peak that the data seem to indicate [25, 26].

2.3. Cosmic Parameters from Current LSS plus CMB Data

Combining LSS and CMB data gives more powerful discrimination among the theories, as Fig. 1 illustrates visually. The approach we used in [4] to add LSS information to the CMB likelihood functions was to design prior probabilities for $\Gamma + \nu_s/2$ and $\sigma_8 \Omega_{nr}^{0.56}$, reflecting the current observations, but with flexible and generous non-Gaussian and asymmetric forms to ensure the priors can encompass possible systematic problems in the LSS data. For example, our choice for $\sigma_8 \Omega_{nr}^{0.56}$ was relatively flat over the 0.45 to 0.65 range.

Using all of the current CMB data and the LSS priors, for the 13 Gyr ΛCDM sequence with gravity waves included, we get $n_s = 1.00^{+.05}_{-.03}$ and $H_0 = 72 \pm 3$ ($\Omega_\Lambda \approx 0.7$), respectively, when H_0 and n_s are marginalized; with no gravity waves, $0.96^{+.07}_{-.05}$ and $H_0 = 70 \pm 3$ are obtained; and for an hΛCDM sequence, with a fixed ratio $\Omega_{hdm}/\Omega_{nr} = 0.2$ for two degenerate massive neutrino species, $n_s \approx 0.97^{+.02}_{-.02}$ and $H_0 \approx 57^{+5}_{-3}$ are obtained, revealing a slight preference for $\Omega_\Lambda \sim 0.3$. For the 15 Gyr ΛCDM sequence, the tilts remain nearly scale invariant and Ω_Λ near 0.6: $0.98^{+.04}_{-.03}$ and $H_0 = 57 \pm 3$ ($\Omega_\Lambda \approx 0.6$) with gravity waves, $0.95^{+.05}_{-.05}$ and 54 ± 3 ($\Omega_\Lambda \approx 0.5$) without.

For the 13 Gyr oCDM sequence, the likelihood peak for the CMB+LSS data is shifted relative to using the CMB data alone because the best fit CMB-only models have σ_8 too low compared with the cluster abundance requirements. Although the $H_0 \approx 54^{+1}_{-1}$ value ($\Omega_{tot} \approx 0.6$) is close to the CMB-only one, the maximum likelihood is significantly below the ΛCDM one. H_0 is larger for the 11 Gyr oCDM sequence, but Ω_{tot} is about the same, and the likelihood is still low.

Should these small error bars be taken seriously? I would be rather surprised if σ_8 from cluster abundances is drastically revised; and as we have seen, the DMR results are quite robust. Although largely driven by just the DMR plus LSS results, the smaller angle CMB results help to fix the tilt, and as the CMB data improves some adjustment might occur, but not a drastic one unless we have made a major

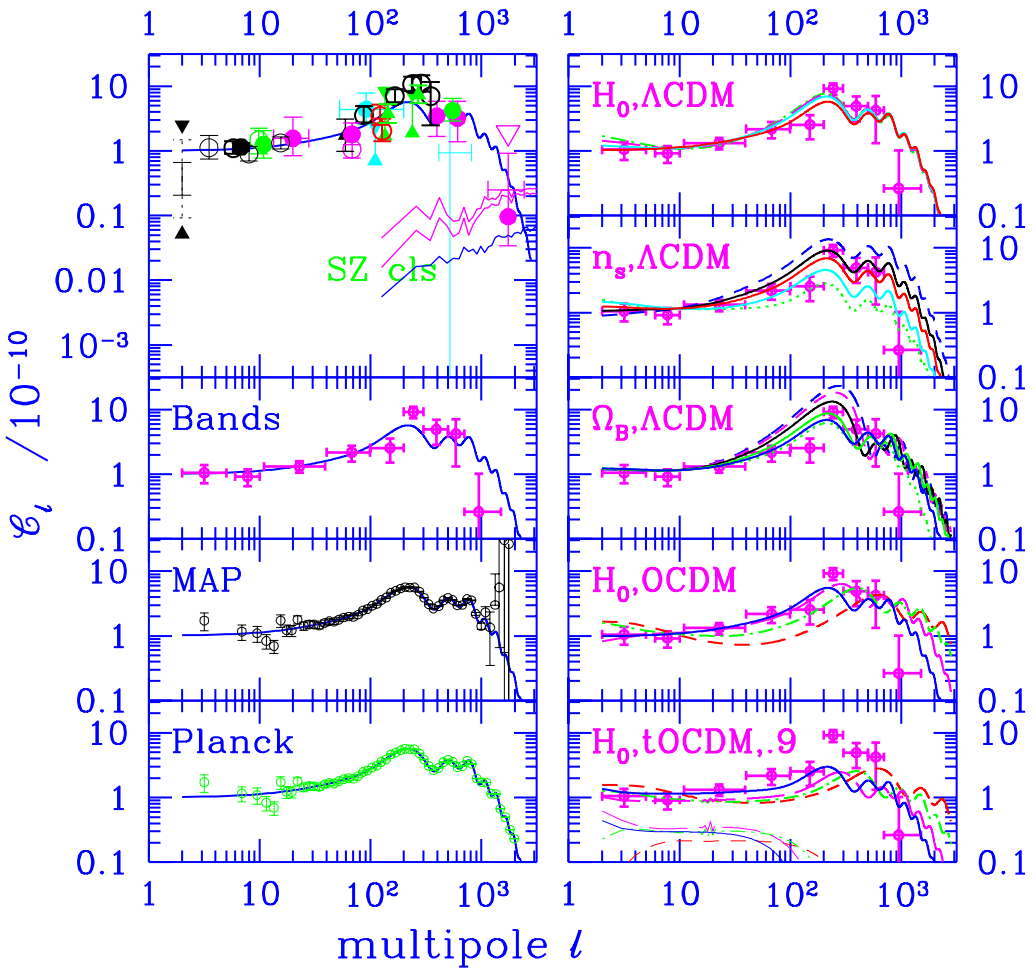

Figure 3. The anisotropy data for experiments up to March 1998 (upper left panel) are compared with secondary $\mathcal{C}_\ell$'s (upper panel) and various primary $\mathcal{C}_\ell$ sequences. The data is optimally combined into 9 bandpower estimates (with one-sigma errors) shown in the next left panel to simplify the comparisons shown in the right panels. To guide the eye an untilted COBE-normalized sCDM model is repeated in all panels. In the two lower left panels, forecasts of how accurate $\mathcal{C}_\ell$ will be determined for this model from the satellites MAP and Planck are shown. The right panels are sequences of 13 Gyr models with variations in: (1) H_0 from 50 to 90, Ω_Λ, 0 to 0.87, for an untilted ΛCDM sequence; (2) n_s from 0.85 to 1.25 for the $H_0 = 70$ ΛCDM model ($\Omega_\Lambda = .66$); (3) $\Omega_B h^2$ from 0.003 to 0.05 for the $H_0 = 70$ ΛCDM model; (4) H_0 from 50 to 65, Ω_k from 0 to 0.84 for the untilted oCDM sequence; (5) the same for a $n_s = 0.9$ oCDM sequence, clearly at odds with the data. The top left panel is extended to low values to show the magnitude of secondary fluctuations from the thermal SZ effect for the ΛCDM and oCDM models (higher curves) and a cluster-normalized sCDM model (lower curve). The kinematic SZ $\mathcal{C}_\ell$ is significantly lower in all cases. Dusty emission from early galaxies may lead to high signals, but the power is concentrated at higher ℓ, with possibly a weak tail because galaxies are correlated extending into the $\ell \lesssim 2000$ regime.

misinterpretation in the nature of the CMB signals observed at intermediate angles.

2.4. Cosmic Parameters from the CMB Future

The expected error bars on the power spectrum from MAP and Planck [21, 30] shown in Fig. 3 illustrate that even quite small differences in the theoretical $\mathcal{C}_\ell$'s and thus the parameters can be distinguished. Quite an industry has developed forecasting how well future balloon experiments (Maxima, Boomerang, ACE, Beast, Top Hat), interferometers (VSA, CBI, VCA) and especially the satellites MAP and Planck could do in measuring the radiation power spectrum and cosmological parameters if foreground contamination is ignored [27, 28, 29, 15, 30, 31, 32]. These have been quite influential in making the case for MAP and Planck.

Table 1 gives some examples of what can be obtained using only CMB data [30]. The temperature anisotropies were assumed to be Gaussian-distributed, and among the > 17 parameters of § 1.3, a restricted 9 parameter space was used: 5 densities, $\{\Omega_B, \Omega_{nr}, \Omega_{hdm}, \Omega_k, \Omega_\Lambda\}\mathrm{h}^2$, the Compton depth τ_C, the scalar tilt, n_s, the total bandpower for the experiment $\langle \mathcal{C}_\ell \rangle_B$ in place of $\mathcal{P}_\Phi(k_n)$, and the ratio of tensor to scalar quadrupole powers, $r_{ts} \equiv \mathcal{C}_2^{(T)}/\mathcal{C}_2^{(S)}$, in place of ν_t. Just like $\mathcal{P}_{GW}/\mathcal{P}_\Phi$, r_{ts} is a sensitive function of ν_t, but also depends on $\nu_s - \nu_t$, Ω_Λ, etc. [1]. In this space, recall that $\mathrm{h}^2 = \sum_j (\Omega_j \mathrm{h}^2)$ is a dependent quantity.

Except for the integrated Sachs-Wolfe effect at low ℓ, the angular pattern of CMB anisotropies now is a direct map of the projected spatial pattern at redshift ~ 100, dependent upon the cosmological angle-distance relation, which is constant along a line relating $\Omega_k \mathrm{h}^2$ and $\Omega_\Lambda \mathrm{h}^2$ for fixed $\Omega_{nr}\mathrm{h}^2$. This defines a near-degeneracy between Ω_k and Ω_Λ broken only at low ℓ where the large cosmic variance precludes accurate determination of both parameters simultaneously. Other cosmological observables are needed to break this degeneracy. A good example is Type I supernovae. If they are assumed to be "standard candles", then their degeneracy is along lines of equal luminosity-distance, which is sufficiently different from the equal angle-distance lines to allow good separate determination.

If the polarization power spectrum can be measured with reasonable accuracy, errors on some parameter such as r_{ts} would improve [31]. However the polarization power spectrum is about a hundred times lower than the total anisotropy, and the gravity wave induced polarization is substantially tinier than this at the low ℓ needed for r_{ts} improvement. We do not know if the foreground polarization will hopelessly swamp this signal.

Error forecasts do depend upon the correct underlying theory. In Table 1, untilted sCDM was chosen as the target model, but the values shown are indicative of what we obtain with other targets [30]. The third column gives errors forecasted for balloon experiments, the bolometer-based TopHat [33], Boomerang [34] and MAXIMA [35] and the HEMT-based BEAST [36]. ℓ-cuts were included to reflect the limited sky coverage these experiments will have. Adding DMR to extend the ℓ-baseline diminishes the forecasted errors.

We adopt the current beam sizes and sensitivities for MAP [14] and Planck [15], improvements over the original proposal values. Of the 5 HEMT channels for MAP, we assume the 3 highest frequency channels, at 40, 60 and 90 GHz, will be dominated by the primary cosmological signal (with 30 and 22 GHz channels partly contaminated by bremsstrahlung and synchrotron emission). MAP also assumes 2 years of observing. For Planck, we use 14 months of observing, the 100, 65, 44 GHz channels for the

Param	Current range	MaxTHBoom +BeastI+dmr	MAP	Planck LFI	Planck HFI
f_{sky}		0.07	0.67	0.67	0.67
δn_s	(0.5–1.5)	.07	.04	.01	.006
δr_{ts}	(0–1)	.55	.24	.13	.09
$\delta\Omega_b h^2/\Omega_b {h_0}^2$	(0.01–0.03)	.11	.05	.016	.006
$\delta\Omega_m h^2/{h_0}^2$	(.2-1)	.20	.10	.04	.02
$\delta\Omega_\Lambda h^2/{h_0}^2$	(0–0.8)	.46	.28	.14	.05
$\delta\Omega_{hdm} h^2/{h_0}^2$	(0–0.3)	.14	.05	.04	.02
τ_C	(0.01–1)	.26	.19	.18	.16
$\delta h/h$	(40–80)	.15	.11	.06	.02
$\delta\Omega_k h^2/{h_0}^2$	(0.2–1.5)	.06	.04	.02	.007
Orthogonal Parameter Combinations within ε					
$\varepsilon < 0.01$	0/9	2/9	3/9	3/9	5/9
$\varepsilon < 0.1$	1/9	6/9	6/9	6/9	7/9

Table 1. Sample idealized MAP and Planck parameter error forecasts, for a 9 parameter inflation family of models, with standard CDM the "Target Model". $\Omega_\Lambda h^2$ is determined with $\Omega_k h^2$ fixed, and $\Omega_k h^2$ is determined with $\Omega_\Lambda h^2$ fixed, because of the angle-distance near-degeneracy; the other parameters are insensitive to fixing either, or neither. The ranges for H_0, $\Omega_B h^2$ are absolute, but the errors are relative ones. The forecasted errors obviously represent a great leap forward from current errors and from what is conceivable with non-CMB probes. Amplitude parameters are highly correlated with τ_C, but this can be partly broken when other information from the abundance of clusters for example is included. The third column is a highly optimistic forecast of what one can do with balloons by combining MAXIMA, TopHat, Boomerang and BeastI with DMR. TopHat, Boomerang, and BeastI would be long duration balloon flights, lasting about a week over the antarctic. It is unclear how well they will do in practice. The specific choices for MAP and Planck are described in the text.

HEMT-based LFI (but not the 30 GHz channel), and the 100, 150, 220 and 350 GHz channels for the bolometer-based HFI (but not the dust-monitoring 550 and 850 GHz channels). The highest resolution for MAP is $13'$ *fwhm*, the highest for Planck is $4'$.

These idealized error forecasts do not take into account the cost of separating the many components expected in the data, in particular Galactic and extragalactic foregrounds, but there is currently optimism that the Galactic foregrounds at least may not be a severe problem e.g., [14, 15], although low frequency emission near 100 GHz by small spinning dust grains [18, 19] may emerge as a new significant source. There is more uncertainty about the extragalactic contributions in the submm and radio.

We forecast that not far away there will be a day when phenomenological theorists will have optimally-analyzed LDBs/VSA/CBI/VCA/MAP/Planck and delivered the power spectrum and cosmic parameters to wonderful precision. What will it mean? It may not be clear. Take inflation as an example. There will be (optimal) attempts to reconstruct the inflaton's potential, but all of our CMB and LSS observations actually access only a very small region of the potential, and even this will be fuzzily determined if we allow too much freedom in parameter space [38]. Still even a fuzzy glimpse is worth the effort. And if the phenomenology teaches us that non-baroque inflation and defect models fail, the CMB and LSS data will be called upon to guide us to a new theory of how fluctuations are generated. Perhaps this will involve interesting topological structure for our observable universe.

References

[1] Bond J R 1996 in *Cosmology and Large Scale Structure*, Les Houches Session LX, August 1993, eds. R. Schaeffer J. Silk, M. Spiro and J. Zinn-Justin (Elsevier Science Press, Amsterdam), pp. 469-674.

[2] Bond J R 1994 in *Relativistic Cosmology*, Proc. 8th Nishinomiya-Yukawa Memorial Symposium, ed. M. Sasaki, (Universal Academy Press, Tokyo), pp. 23.

[3] Bennett C, Banday A J, Gorski K M, Hinshaw G, Jackson P, Keegstra P, Kogut A, Smoot G F, Wilkinson D T, Wright E L 1996 Ap. J. Lett. **464**, 1.

[4] Bond J R and Jaffe A 1996 in *Microwave Background Anisotropies*, Proceedings of the XXXI Rencontre de Moriond, ed. Bouchet, F R, Edition Frontières, Paris, pp. 197, astro-ph/9610091; 1998 CITA preprint.

[5] Peacock J A 1997 M.N.R.A.S. **284**, 885.

[6] Lidsey J E, Liddle A R, Kolb E W, Copeland E J, Barreiro T and Abney M 1997 RMP **69**, 373.

[7] Hu W, Sugiyama N and Silk J 1997 Nature **386**, 37.

[8] Hu W and White M 1997, New Astron **2**, 323.

[9] Bertschinger E, Bode P, Bond J R, Coulson D, Crittenden R, Dodelson S, Efstathiou G, Gorski K, Hu W, Knox L, Lithwick Y, Scott D, Seljak U, Stebbins A, Steinhardt P, Stompor R, Souradeep T, Sugiyama N, Turok N, Vittorio N, White M, Zaldarriaga M 1995 ITP workshop on *Cosmic Radiation Backgrounds and the Formation of Galaxies*, Santa Barbara.

[10] Seljak U and Zaldarriaga M 1996 Ap. J. **469**, 437.

[11] Fixsen D J, Cheng E S, Gales J M, Mather J C, Shafer R A and Wright E L 1997 Ap. J. **473**, 576.

[12] Bond J R and Myers S 1996 Ap. J. Supp. **103**, 1-79.

[13] Netterfield C B, Devlin M J, Jarosik N, Page L and Wollack E J 1997 Ap. J. **474**, 47.

[14] MAP experiment home page, http://map.gsfc.nasa.gov

[15] Bersanelli M, Bouchet F R, Efstathiou G, Griffin M, Lamarre J M, Mandolesi N, Norgaard-Nielson H U, Pace O, Polny J, Puget J L, Tauber J, Vittorio N and Volonte S 1996 COBRAS/SAMBA, The Phase A Study for an ESA M3 Mission, preprint; Planck home page, http://astro.estec.esa.nl/SA-general/Projects/Cobras/cobras.html

[16] Gundersen J O, Lim M, Staren J, Wuensche C A, Figueiredo N, Gaier T C, Koch T, Meinhold P R, Seiffert M D, Cook G, Segale A and Lubin P M 1995 Ap. J. Lett. **443**, L57.

[17] Netterfield C B, Jarosik N, Page L and Wilkinson D 1995 Ap. J. Lett. **455**, L69.

[18] Leitch E M, Readhead A C S, Pearson T J and Myers S T 1997 Ap. J. Lett. **486**, 23.

[19] Draine B T and Lazarian A 1998 Ap. J. Lett. **494**, 19.

[20] Jaffe A H, Knox L and Bond J R 1997 preprint astro-ph/9702109; 1998 preprint.

[21] Bond J R, Jaffe A H and Knox L 1998 Phys. Rev. D **57**, 2117.

[22] Chaboyer B, Demarque P, Krauss L M and Kernan P J 1998 Ap. J. **494**, 96.

[23] Bond J R, Pogosyan D and Souradeep T 1997 preprint astro-ph/9702212; 1998 this volume; 1998 preprint.

[24] Cornish N J, Spergel D N and Starkman G D 1996 *preprint* gr-qc/9602039; 1998, this volume; Levin J J, Barrow J D, Bunn E F and Silk J 1997 *Phys. Rev. Lett.* **79** 974; Levin J J, Scannapieco E and Silk J 1998, this volume.

[25] Pen Ue-Li, Seljak U and Turok N 1997 Phys. Rev. Lett. **79**, 1611-1614.

[26] Allen B, Caldwell R R, Dodelson S, Knox L, Shellard E P S and Stebbins A 1997 preprint astro-ph/9704160.

[27] Knox L 1995 Phys. Rev. D **52**, 4307.

[28] Tegmark M and Efstathiou G 1996 M.N.R.A.S. 281, 1297.

[29] Jungman G, Kamionkowski M, Kosowsky A and Spergel D N 1996 Phys. Rev. Lett. **76**, 1007.

[30] Bond J R, Efstathiou G and Tegmark M 1997 M.N.R.A.S. **291**, L33.

[31] Zaldarriaga M, Spergel D and Seljak U 1997 Ap. J. **488**, 1.

[32] White M, Carlstrom J E and Dragovan M 1997, astro-ph/9712195

[33] TopHat home page, http://cobi.gsfc.nasa.gov/msam-tophat.html

[34] Boomerang home page, http://astro.caltech.edu/ mc/boom/boom.html

[35] MAXIMA home page, http://physics7.berkeley.edu/group/cmb/gen.html

[36] ACE/Beast home page, http://www.deepspace.ucsb.edu/research/Sphome.html

[37] Lineweaver C and Barbosa D 1997 astro-ph/9706077; Hancock S and Rocha G 1997, astro-ph/9612016, in *Proceedings of the XVIth Moriond meeting, "Microwave Background Anisotropies,"* ed. F R Bouchet et al. (Gif-Sur-Yvette: Editions Frontières).

[38] Souradeep, T, Bond J R, Knox L, Efstathiou G and Turner M S 1998 astro-ph/9802262